INTERNATIONAL JOURNAL FOR NUMERICAL METHODS IN FLUIDS, VOL. 13, 955–970 (1991)

A CONTROL VOLUME FINITE ELEMENT METHOD FOR THREE-DIMENSIONAL NAPL GROUNDWATER CONTAMINATION

F. W. LETNIOWSKI

Nova Corporation of Alberta, Calgary, Alberta, T2P 2N6, Canada

AND

P. A. FORSYTH

Department of Computer Science, University of Waterloo, Waterloo, Ontario, N2L 3G1, Canada

SUMMARY

A three-dimensional control volume finite element method is developed for NAPL groundwater contamination problems. Tetrahedral elements are formed by decomposing deformed blocks. The decomposition is carried out in such a way as to minimize the size of the negative transmissibilities. Negative transmissibilities produce non-physical discrete fluid flow paths and can cause oscillatory behaviour in the Newton iteration. Example results are presented for a three-dimensional NAPL contamination scenario using typical geophysical data.

KEY WORDS Three-dimensional tetrahedral NAPL contamination

1. INTRODUCTION

Groundwater contamination by non-aqueous phase hazardous substances is a problem of growing concern.[1-9] Compounds such as creosote, TCE and gasoline are examples of toxic substances which form a non-aqueous phase. These substances are commonly referred to as NAPL (non-aqueous phase liquid) contaminants. Decommissioned petrochemical plants and abandoned town gas production facilities are examples of sources of NAPL contaminants.

Simulation of NAPL contaminant flow requires the solution of three-phase flow in a porous medium.[3,10,11] In groundwater applications it is common to invoke the passive air phase approximation.[3,12] This approach results in numerical solution of a three-phase problem having computational requirements similar to a two-phase simulation.

Various techniques have been devised for modelling NAPL contamination. These methods include two-dimensional finite difference[1,3-6] and finite element methods.[8,9] Three-dimensional finite difference methods have also been devised.[7]

Since adjacent geological layers can have an order-of-magnitude difference in physical properties, it is convenient to place grid nodes in locations which correspond to these layers. In practice, these layers are rarely planes. Consequently, the resulting grid is irregular.

The basic discretization method which will be used in the following is essentially a finite volume approach with finite-element-type basis functions. This has variously been described as a control

0271–2091/91/180955–16$08.00

Received 23 March 1990
Revised 19 December 1990

volume–finite element method,[13,14] the box method[15] or the influence coefficient technique.[16] This method combines the flexibility of a finite element method with the local conservation property and easy identification of upstream points characteristic of finite difference methods.[11] Owing to the non-linear hyperbolic nature of the equations (in the limit of zero capillary pressure), upstream weighting is required to ensure convergence to the physically correct solution which satisfies the entropy condition.[17]

In a previous paper,[18] two-dimensional problems were solved using a triangular grid with first degree C^0 (linear) basis functions. Typically, geophysical problems have the horizontal dimension much larger than the vertical dimension. In this case, first-degree C^0 Lagrange basis functions defined on quadrilaterals are inappropriate, since a large number of 'negative transmissibilities' are obtained in the discretization process. This is physically undesirable, since negative transmissibilities result in a discrete fluid flow which is in the opposite direction to the physical fluid flow.

Violation of the positive transmissibility condition for unsaturated flow problems may not be too serious. However, in the case of multiphase flow, with mobile fluids of differing densities, negative transmissibilities produce demonstrably poor results. As an example, consider the following situation: suppose that node A is physically located above node B (depth increasing as we move from A to B). At the initial instant in time let both nodes A and B contain mobile saturations of a dense fluid and a light fluid. Owing to buoyancy forces, the dense fluid should move from A to B while the light fluid should move from B to A. The discretized system will demonstrate this behaviour if the transmissibility between A and B is positive. However, if the transmissibility between A and B is negative, then the discrete solution will show that the dense fluid 'floats' on top of the light fluid. This pathological behaviour has been demonstrated computationally in Reference 18.

Of course, it can be argued that such observable non-physical behaviour is extremely rare. However, even in cases where the discrete solution does not demonstrate non-physical behaviour, negative transmissibilities may cause poor convergence behaviour of the Newton iteration. Some examples of this effect will be given in this paper.

In the case of a constant permeability tensor a given set of nodes in two dimensions can be triangulated so that all interior edges have positive transmissibilities. This is possible in two dimensions because of the equivalence of the positive transmissibility condition and a Delauney triangulation.[19] Briefly, a Delauney triangulation satisfies the empty circle criterion: the circumcircle of any triangle in a Delauney triangulation contains no other nodes in its interior.[19] More generally, for a non-constant permeability tensor computational experiments indicate that a generalized Delauney edge swap algorithm produces only a small number of negative transmissibilities.[18]

The objective of this work is to consider full three-dimensional discretizations. The natural extension of triangular basis functions to three dimensions results in the use of tetrahedral elements.

Unfortunately, a three-dimensional Delauney triangulation does not, in general, produce positive transmissibilities.[20] Moreover, it can be shown that positive transmissibilities cannot be obtained, in general, by transformations of tetrahedral faces.[20] Consequently, it is not possible to obtain positive transmissibilities in three dimensions without node movement.

Of course, it is still possible to seek a triangulation which minimizes the number and size of the negative transmissibilities. In this paper we will demonstrate the use of a straightforward heuristic technique for constructing a grid composed of tetrahedra, which is suitable for geophysical applications. This method produces negative transmissibilities which are small in size. The importance of having small negative transmissibilities is demonstrated by solving a model

problem with two grids. These grids have identical node locations but use different triangulations. One of the triangulations has large negative transmissibilities, which results in extremely poor computational performance.

Some example results for a realistic NAPL contamination problem are also given and we discuss the numerical problems associated with NAPL simulation.

2. MODEL EQUATIONS

The three phases which appear in NAPL contamination models are water (w), air (a) and NAPL (n). If the passive air phase approximation is used, then the following equations hold:

water conservation,

$$\frac{\partial}{\partial t}(\phi\rho_w S_w)=\rho_w q'_w+\nabla\cdot[\mathbf{K}\rho_w\lambda_w(\nabla P_w-\rho_w g\nabla D)], \tag{1}$$

NAPL conservation,

$$\frac{\partial}{\partial t}(\phi\rho_n S_n)=\rho_n q'_n+\nabla\cdot[\mathbf{K}\rho_n\lambda_n(\nabla P_n-\rho_n g\nabla D)], \tag{2}$$

where S_l is the saturation of phase l, ϕ is the porosity, $\lambda_l=K_{rl}/\mu_l$, K_{rl} is the relative permeability of phase l, μ_l is the viscosity of phase l, $\mathbf{K}$ is the absolute permeability tensor, D is the depth, g is the gravitational acceleration, P_l is the pressure of phase l, ρ_l is the density of phase l and q'_l is the source/sink term for phase l. In addition, we have the following constraints:

$$S_n+S_a+S_w=1, \tag{3}$$

$$P_a=P_n+\alpha P_{can}(S_a)+(1-\alpha)[P_{caw}(S_a)-P_{cnw}(S_w=1)], \tag{4}$$

$$P_n=P_w+\alpha P_{cnw}(S_w)+(1-\alpha)P_{cnw}(S_w=1), \tag{5}$$

where

$$\alpha=\min(1, S_n/S_n^*) \tag{6}$$

and P_{can}, P_{cnw} and P_{caw} are experimentally determined capillary pressure curves, as are the relative permeability curves K_{rl}.[10,11] Equations (3)–(6) ensure that the capillary pressures have the correct limits as $S_n\to 0$. S_n^* is a blending parameter.[18] Assuming that the air pressure P_a is constant, then equations (1)–(5) represent a system of five equations in the five unknowns

$$P_n,\quad P_w,\quad S_n,\quad S_w,\quad S_a. \tag{7}$$

The constraint equations (3)–(5) can be used to eliminate three unknowns, so that two primary unknowns remain. In the following the primary unknowns are selected to be (S_n, P_n).

3. DISCRETIZATION

We illustrate the discretization method for equation (2). In the following, superscripts N, $N+1$ and M represent time levels. A quantity with superscript M may be a function of several variables, some of which are evaluated at time level $N+1$ and some of which are evaluated at time level M. For example,

$$\lambda_w^M=\lambda_w(P_n^{N+1}, S_n^M). \tag{8}$$

This will be explained in detail below.

Let $\mathbf{N}_i$ be the usual Lagrange polynomial C^0 basis functions, where

$$\mathbf{N}_i = \begin{cases} 1 & \text{at node } i, \\ 0 & \text{at all other nodes,} \end{cases} \tag{9}$$

$$\sum_j \mathbf{N}_j = 1 \quad \text{everywhere in the solution region.}$$

Let

$$P_n = \sum_j P_{nj}\mathbf{N}_j,$$

$$\psi_n = \sum_j (P_{nj} - \rho_{nj} g D_j)\mathbf{N}_j = \sum_j \psi_{nj}\mathbf{N}_j,$$

$$S_n = \sum_j S_{nj}\mathbf{N}_j. \tag{10}$$

If a lumped mass approach is used for the time derivative and a Galerkin approximation is used for the divergence term, then equation (2) becomes (using equation (10))

$$\left(\frac{(\phi\rho_n S_n)_i^{N+1} - (\phi\rho_n S_n)_i^N}{\Delta t}\right)\int_v \mathbf{N}_i \mathrm{d}v = (\rho_n q'_n)_i^{N+1}\int_v \mathbf{N}_i \mathrm{d}v - \int_v \lambda_n^M \rho_n^M \mathbf{K}\nabla\left(\sum_j \psi_{nj}^M \mathbf{N}_j\right)\cdot\nabla\mathbf{N}_i \mathrm{d}v, \tag{11}$$

where the integrals are over the solution domain v and Δt is the time step size.

Using equation (9), we can write

$$\nabla\left(\sum_j \mathbf{N}_j\right) = \nabla\mathbf{N}_i + \sum_{j\neq i}\nabla\mathbf{N}_j = 0. \tag{12}$$

Consequently

$$\nabla\left(\sum_j \psi_{nj}^M \mathbf{N}_j\right) = \psi_{ni}^M \nabla\mathbf{N}_i + \sum_{j\neq i}\psi_{nj}^M\nabla\mathbf{N}_j = \sum_{j\neq i}(\psi_{nj}^M - \psi_{ni}^M)\nabla\mathbf{N}_j. \tag{13}$$

If

$$V_i = \int_v \mathbf{N}_i \mathrm{d}v, \qquad q_{ni} = \rho_{ni} q'_{ni} V_i, \tag{14}$$

then equations (11)–(14) give

$$\frac{V_i}{\Delta t}[(\phi\rho_n S_n)_i^{N+1} - (\phi\rho_n S_n)_i^N] = q_{ni}^{N+1} - \sum_{j\neq i}(\psi_{nj}^M - \psi_{ni}^M)\int_v \lambda_n^M \rho_n^M \mathbf{K}\nabla\mathbf{N}_i\cdot\nabla\mathbf{N}_j \mathrm{d}v. \tag{15}$$

The control volume–finite element method approximates the integral in equation (15) by

$$-\int \lambda_n^M \rho_n^M \mathbf{K}\nabla\mathbf{N}_j\cdot\nabla\mathbf{N}_i \mathrm{d}v \approx (\lambda_n^M \rho_n^M)_{ij}^{\mathrm{ups}}\gamma_{ij}, \tag{16}$$

where

$$\gamma_{ij} = -\int_v \mathbf{K}\nabla\mathbf{N}_j\cdot\nabla\mathbf{N}_i \mathrm{d}v \tag{17}$$

and $(\lambda_n^M \rho_n^M)_{ij}^{\mathrm{ups}}$ is evaluated at the upstream point $\{i,j\}$. (This will be discussed below.) The approximation involved in equation (16) is first-order-correct in regions where $(\lambda_n^M \rho_n^M)$ is non-constant. This is unavoidable if we use upstream weighting for λ_n^M, which is required to

ensure convergence to the correct solution[17] for non-linear λ_n. Of course, if S_n is constant over the support of N_i, then no approximation is involved in equation (16).

Finally, combining equations (15) and (16) gives

$$\frac{V_i}{\Delta t}[(\phi\rho_n S_n)_i^{N+1}-(\phi\rho_n S_n)_i^N]=q_{ni}^{N+1}+\sum_{j\in\eta_i}\gamma_{ij}(\lambda_n^M\rho_n^M)_{ij}^{ups}(\psi_{nj}^M-\psi_{ni}^M), \tag{18}$$

where η_i is the set of neighbour nodes of node i such that γ_{ij} is non-zero.

A similar procedure can be used to discretize the water conservation equation. More precisely, the discrete equations for both water and NAPL are as follows:

water equation,

$$\frac{V_i}{\Delta t}[(\phi\rho_w S_w)_i^{N+1}-(\phi\rho_w S_w)_i^N]=q_{wi}^{N+1}+\sum_{j\in\eta_i}\gamma_{ij}(\lambda_w^M\rho_w^M)_{ij}^{ups}(\psi_{wj}^M-\psi_{wi}^M), \tag{19}$$

where

$$\psi_{wi}^M=P_{ni}^{N+1}-(P'_{cnw,i})^M-\rho_{w,ij+1/2}^M gD_i,$$
$$P'_{cnw}=P_n-P_w \quad \text{(see equation (5))}, \tag{20}$$

NAPL equation,

$$\frac{V_i}{\Delta t}[(\phi\rho_n S_n)_i^{N+1}-(\phi\rho_n S_n)_i^N]=q_{ni}^{N+1}+\sum_{j\in\eta_i}\gamma_{ij}(\lambda_n^M\rho_n^M)_{ij}^{ups}(\psi_{nj}^M-\psi_{ni}^M), \tag{21}$$

where

$$\psi_{ni}^M=P_{ni}^{N+1}-\rho_{n,ij+1/2}^M gD_i \tag{22}$$

and where

$$q_l=q_l'V_i\rho_l, \qquad \lambda_w^M=\lambda_w(P_n^{N+1},S_n^M), \qquad \lambda_n^M=\lambda_n(S_n^M), \tag{23}$$
$$\rho_{l,ij+1/2}=\frac{\rho_{l,i}+\rho_{l,j}}{2}, \qquad (\lambda_l\rho_l)_{ij}^{ups}=\begin{cases}(\lambda_l\rho_l)_i & \text{if } \gamma_{ij}(\psi_{ij}^M-\psi_{ii}^M)<0,\\ (\lambda_l\rho_l)_j & \text{if } \gamma_{ij}(\psi_{ij}^M-\psi_{ii}^M)>0.\end{cases}$$

Allowing M to be either $M=N$ or $M=N+1$ and letting M vary from node to node ($M=M(i)$) defines an adaptive implicit method[21,22] which will be used in the following. Further details concerning the above method can be found in References 21 and 22.

The discrete equations (19) and (21) are solved using full Newton iteration and the Jacobian is solved using an incomplete LU (ILU) factorization with Orthomin acceleration.[23]

4. THE POSITIVE TRANSMISSIBILITY CONDITION

In order to demonstrate the basic idea of positive transmissibilities, consider the simple case of the diffusion equation

$$c_t=\nabla\cdot\mathbf{K}\nabla c \tag{24}$$

where c is the concentration of some chemical and $\mathbf{K}$ is the diffusion tensor. Consider the situation shown in Figure 1. Suppose that at the initial instant in time the concentration profile of c is such that

$$\frac{\partial c}{\partial x}=\text{constant}<0, \qquad \frac{\partial c}{\partial y}=0. \tag{25}$$

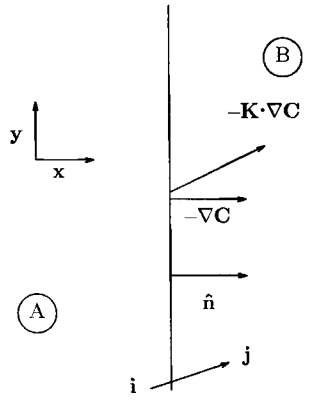

Figure 1. Domain for diffusion equation example

For simplicity we assume that the boundary conditions are zero flux and that the boundaries are far away from the flux surface shown in Figure 1. Consider a flux surface normal to the x-direction. Then (assuming equation (25))

$$\hat{n} = -\frac{\nabla c}{|\nabla c|}$$

and the concentration flux is given by

$$\vec{f} = -\mathbf{K} \cdot \nabla c,$$

so that the flux normal to the surface in Figure 1 is

$$\vec{f} \cdot \hat{n} = \frac{\nabla c \cdot \mathbf{K} \cdot \nabla c}{|\nabla c|} > 0,$$

since $\mathbf{K}$ must be positive definite. Consequently, the diffusive flux is out of region A and into region B.

More concretely, consider two points on either side of the flux surface, i and j (Figure 1). In the above situation it is not possible for the chemical to diffuse from B to A since it would have to cross the surface and the flux at the surface points from A to B. Let

$$c = \sum c_i \mathbf{N}_i,$$

where c_i are the nodal values of the discrete concentration and $\mathbf{N}_i$ are the basis functions as defined in equation (9).

Then, a lumped mass, Galerkin approximation to equation (24) is

$$\left(\frac{c_i^{N+1} - c_i^N}{\Delta t}\right) V_i = \sum_{j \in \eta_i} \gamma_{ij} (c_j^M - c_i^M), \tag{26}$$

where γ_{ij} is given by equation (17), V_i is defined in equation (14), η_i is the set of neighbour nodes of node i, and $M = N$ if an explicit approximation is used, and $M = N + 1$ if an implicit approximation is used.

Suppose an explicit method is used to solve equation (26) ($M=N$). Given the initial state as defined by equation (25), choose a Δt sufficiently small so that equation (26) is stable. From equation (25)

$$c_i^N > c_j^N, \tag{27}$$

where i and j are as in Figure 1, so that the discrete movement of chemical from node j to node i is given by

$$-\Delta t \gamma_{ij} |c_j^N - c_i^N|. \tag{28}$$

If $\gamma_{ij} > 0$, then chemical leaves node i and enters node j. However, if $\gamma_{ij} < 0$, then chemical leaves node j and enters node i, which is not physically possible. Thus in the case of $\gamma_{ij} < 0$ there is a non-physical flux path between node i and node j. Of course, this non-physical path is balanced by other paths, so that the net discrete flux across the surface points in the correct direction. However, it is clear that if $\gamma_{ij} < 0$, some of the discrete flux paths are non-physical.

A more extreme example of the above phenomenon is given by assuming the initial state

$$c_i^N = 1, \qquad c_j^N = 0, \quad \forall j, \quad j \neq i. \tag{29}$$

For a sufficiently small time Δt (from equation (26))

$$c_i^{N+1} = 1 - \frac{\Delta t}{V_i} \sum_{j \in \eta_i} \gamma_{ij}, \qquad c_j^{N+1} = \frac{\Delta t \gamma_{ij}}{V_i}, \quad j \in \eta_i. \tag{30}$$

If $\gamma_{ij} > 0$, $\forall i, j$, then the concentration decreases at node i and increases at node j. However, if $\gamma_{il} < 0$, $l \in \eta_i$, then the concentration of node l becomes less than zero. This violates the maximum principal of the original equation (24).

Alternatively, if an implicit approximation to equation (26) is used, then equation (26) can be written as

$$\mathbf{A} c^{N+1} = \mathbf{V} c^N, \qquad [\mathbf{V}]_{ij} = V_i \delta_{ij}. \tag{31}$$

If $\gamma_{ij} > 0$, then $\mathbf{A}$ is an M-matrix,[24] which implies that

$$\min_j u_j^N \leqslant u_i^{N+1} \leqslant \max_j u_j^N \tag{32}$$

(recall that all boundary conditions are zero flux). Equation (32) is a discrete version of the maximum principal of the original equation (24). Equation (32) is true for any time step and in particular implies that the discrete concentration can never become less than zero if

$$u_i > 0, \quad \forall i,$$

at the initial time. This argument is also independent of mesh size.

If linear basis functions defined on triangles are used, then the condition for $\gamma_{ij} \geqslant 0$ has a simple geometric interpretation if $\mathbf{K} = \mathbf{I}$. If α and β are the two angles opposite an interior edge of the triangulation, then γ_{ij} are positive if[14]

$$\alpha + \beta \leqslant \pi.$$

A Delauney triangulation satisfies this condition for internal edges of the triangulation.[19]

The appearance of small negative concentrations may only be a minor annoyance for the linear diffusion equation. However, for multiphase fluid flow, negative transmissibilities can cause non-physical discrete fluid flow. This is especially true for gravity-dominated systems. As discussed in Section 1, this non-physical flow path can cause the discrete buoyancy forces to act in

the opposite direction to the physical buoyancy forces. This has the computational effect of causing poor convergence behaviour for the Newton iteration. This will be demonstrated in some examples in the following.

5. CHOICE OF BASIS FUNCTIONS AND TRIANGULATION METHOD

As described in Section 1, we would like to produce a discretization such that all transmissibilities are positive, i.e.

$$\gamma_{ij} > 0. \tag{33}$$

In order to eliminate some possibilities, consider for the moment the problem of ensuring that equation (33) is satisfied for a three-dimensional region divided into rectangular blocks or bricks (hexahedral elements), with each face of a hexahedron being perpendicular to other faces. Of course, we could use a finite difference method for this type of grid to ensure that equation (33) is satisfied. However, it is difficult to generalize a finite difference method to more irregular geometries. Irregular meshes in the finite element case can be constructed by distorting the blocks.

A natural choice for hexahedral elements are C^0 Lagrangian basis functions (tensor products of one-dimensional linear basis functions). Consider the case of a constant, isotropic permeability tensor $\mathbf{K}$. If Δx, Δy and Δz are the physical dimensions of the block, then in geophysical applications Δz is typically much smaller than either Δy or Δx. In this case some straightforward algebra (equation (17)) shows that horizontal transmissibilities are negative, even if $\Delta x = \Delta y$. Consequently, if our criterion is to minimize the possibility of negative transmissibilities, then C^0 Lagrangian hexahedral basis functions are inappropriate.

The simplest choice of three-dimensional elements uses first-degree C^0 linear basis functions defined on tetrahedra. These are the natural extension of two-dimensional first-degree C^0 Lagrange triangular basis functions. In two dimensions all interior transmissibilities will be positive if the nodes are connected by a two-dimensional Delauney triangulation.[18] Unfortunately, Delauney triangulations in three dimensions do not, in general, produce positive transmissibilities.[20] In fact, it is not possible, in general, to eliminate interior negative transmissibilities in three dimensions.[20] Consequently, we seek only to minimize the size and number of the negative transmissibilities.

Three-dimensional blocks can be divided into tetrahedra in essentially two ways. Either five tetrahedra can be used, as shown in Figure 2, or six tetrahedra, as in Figure 3.

The five tetrahedra in Figure 2 are ABDF, ACDG, ADFG, AEFG and DFGH. The six tetrahedra in Figure 3 are ABDH, ABFH, ACDH, ACGH, AEFH and AEGH.

Assuming that $\mathbf{K}$ is constant and isotropic, it is easy to show that the six-tetrahedra configuration produces zero diagonal transmissibilities and positive block edge transmissibilities. In fact, the six-tetrahedra configuration reduces to the common seven-point finite difference molecule.

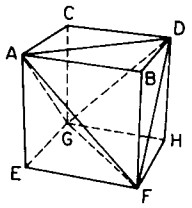

Figure 2. Five-tetrahedra decomposition of a rectangular block

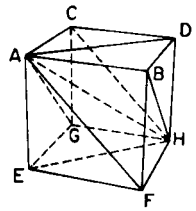

Figure 3. Six-tetrahedra decomposition of a rectangular block

For the five-tetrahedra configuration the block edge transmissibilities are positive but the (interior) diagonal transmissibilities may be negative. The diagonal transmissibilities have the form

$$\gamma_{ij}(\text{diagonal}) = \frac{1}{12}\Delta x \Delta y \Delta z \left(\frac{1}{\Delta x^2} + \frac{1}{\Delta y^2} - \frac{1}{\Delta z^2} \right), \tag{34}$$

where Δx, Δy and Δz are cyclically permuted depending on which diagonal is being evaluated. Note that if Δz is small compared to Δx and Δy, then equation (34) is negative.

A straightforward technique can be used to construct tetrahedral grids. This method is particularly suited to geophysical problems. First, a two-dimensional grid of quadrilaterals is defined on the physical surface (the top layer). The third dimension of the problem can be constructed by specifying the z-co-ordinate of each surface point and by giving the z-co-ordinate of each point in the layers below that surface point. A stratified porous medium automatically lends itself to this approach. Also, field data are commonly available in this form. For example, geological data are often displayed in terms of contour maps showing depths to layers and layer thicknesses.

This technique conveniently defines deformed blocks, which may then be divided into tetrahedra. Note that the deformed blocks no longer have planar surfaces, since the four points on a block face will not, in general, form a plane. For example, in Figures 2 and 3 ACD could form one plane and ABD would form another plane.

In the above we have assumed that the projection of the grid on each layer onto the x–y plane is the same. However, this technique can be generalized to any set of quadrilateral grids such that each grid is isomorphic to the grid above (or below) it. In other words, each grid on a given layer can be transformed by a sequence of stretching and pulling operations into the grid above (below) it.

6. LNAPL EXAMPLE

The first example is an extension of the problem solved by Faust[1] and others.[6] The original problem is a two-dimensional x–z cross-sectional LNAPL (light non-aqueous phase liquid, with density of NAPL less than density of water) scenario. The model was extended to three dimensions by using nodes a unit distance apart in the y-direction.

In essence, the problem has been made three-dimensional by connecting two identical cross-sections together. This is trivially three-dimensional, since the results should be the same on each two-dimensional cross-section. However, this example provides a convenient verification of the three-dimensional discretization technique, since the numerical solution is well known. It also provides a useful problem to test the five- and six-tetrahedra block decomposition methods.

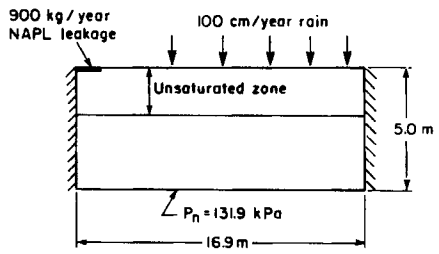

Figure 4. Domain for the Faust[1] problem

The original problem[1] was posed on a cell-centred finite difference grid. In other words, the finite volumes are blocks, where values are taken at the block centres. The control volume–finite element method is applied by defining nodes at the vertices of the cells. This results in a two-dimensional cross-section of 7×21 nodes, compared to the original 6×20 grid. Figure 4 shows the problem domain. Complete details of the data used for this problem are given in Reference 1 and will not be repeated here.

This problem was solved using both the five- and six-tetrahedra methods for block decomposition. The run statistics for both computations are reported in Table I. The five-tetrahedra run failed to reach the end time before the CPU time limit expired. At this point the five tetrahedra discretization had consumed more than 10 times the CPU time of the six-tetrahedra method.

The total CPU time is proportional to both the total number of Newton iterations and the number of non-zero transmissibilities. Table I indicates that the five-tetrahedra configuration has twice as many non-zero transmissibilities and requires five times as many Newton iterations as the six-tetrahedra method. Consequently, we expect that the five-tetrahedra discretization will require an order of magnitude more CPU time, as is observed.

We emphasize that the only difference between these two computations is the method for decomposing blocks into tetrahedra. All other data were identical. The five-tetrahedra formulation had many repeat times teps owing to failure of the Newton iteration.

A detailed analysis of the Newton iteration for the five-tetrahedra decomposition revealed an interesting physical explanation for the convergence failures. As described previously, the five-tetrahedra discretization procedure produces positive transmissibilities along a block edge, while diagonal transmissibilities are negative. Physically, for this example, the LNAPL sinks down through the unsaturated zone until the water table is encountered. Consequently, during a

Table I. Computational statistics for the tetrahedra discretizations, Faust problem[1]

	Six tetrahedra	Five tetrahedra
Normalized CPU time	1·0	12·7*
Newton iterations	60	335*
Time reached	390·55 days	183 days*
Material balance error	2×10^{-5}	6×10^{-5}*
Number of time steps	10	30*
Non-zero transmissibilities	679	1185
Negative transmissibilities	0	114

* Failed to reach stopping time before CPU time limit expired.

Table II. Computational statistics for the tetrahedra discretizations, variable layer depth Faust problem

	Six tetrahedra	Five tetrahedra
Normalized CPU time	1·0	3.5
Newton iterations	63	163
Time reached	390·55 days	390·55 days
Material balance error	5×10^{-5}	4×10^{-4}
Number of time steps	11	17
Repeated time steps	0	6
Non-zero transmissibilities	1298	1185
Negative transmissibilities	259	126
Maximum size of negative transmissibilities	10^{-14} m	10^{-12} m

Newton iteration, liquid flows down the edge of a block but then flows back up along the negative transmissibility, i.e. in the negative physical flow direction. The next Newton iteration attempts to correct this by sending more fluid down the edge of the block. This is repeated until eventually a solution is reached. When the negative connection is large, this process may continue indefinitely (if the time step is large). Consequently, the five-tetrahedra formulation results in many repeat time steps.

It could be argued that the case of a hexadron with perpendicular sides is atypical, since the six-tetrahedra decomposition has no negative transmissibilities. To verify that the superior performance of the six-tetrahedra discretization is not just restricted to unusual cases, the Faust LNAPL problem was perturbed slightly. The z-co-ordinate was given an average dip of approximately 3% in the x-direction. In other words, differences in the depths of nodes in the same layer were approximately 3% of their horizontal separation. Consequently, the blocks are not quite rectangular.

The computational statistics for this variable layer depth Faust problem are given in Table II. Note that now the six-tetrahedra formulation has more negative transmissibilities than the five-tetrahedra decomposition, but the maximum absolute size of the negative transmissibility is 100 times smaller. The results indicate that, once again, the six-tetrahedra formulation is more computationally efficient than the five-tetrahedra decomposition. Table II suggests that the absolute size of the negative transmissibilities may be more important than the number of negative transmissibilities.

7. FULL THREE-DIMENSIONAL DNAPL EXAMPLE

This example is a full three-dimensional simulation of dense NAPL (DNAPL) contamination using typical geophysical and fluid data.

A $25 \times 13 \times 10$ grid of deformed blocks was used. In the light of the results of the previous section, these blocks were decomposed into six tetrahedra. A rectangular 25×13 grid was used in the horizontal (x–y) plane. The physical size of the x–y plane was $240 \times 120\ \text{m}^2$, with a node spacing in the x- and y-directions of 10 m. The depth of the lowermost layer (layer 10) varied from about 50 to 60 m.

No-flow boundaries were used on all domain edges, except the $x=0$ plane, the $x=240$ m plane and the surface. At $x=0$ the water table was assumed to lie at a depth of 2 m (constant in the y-direction). At $x=240$ m the water table was at a depth of 6 m. The water pressure at the water

table was taken to be 100 kPa and a hydrostatic boundary condition was used below the water table. A constant air pressure boundary is used at the surface.[6]

DNAPL was considered to be leaking at the surface from a distributed source spread over an area of $10 \times 20\ m^2$ (nodes (4, 6) and (4, 7)). The total leakage rate was assumed to be $100\ m^3\ year^{-1}$.

Other data for this problem are given in Tables III and IV. Note that the absolute permeabilities vary by eight orders of magnitude. This is not uncommon for geophysical problems and provides a severe test for the iterative Jacobian solver.

This problem was run to a simulated time of 5 years. The run statistics are given in Table V. On average, about seven Newton iterations were required per time step, indicating the severe non-linearity of this problem. Approximately five iterations of the incomplete factorization iterative solver were required for each Jacobian solved. This indicates that the iterative solver performed quite well in spite of the large permeability contrasts. A reduced system incomplete LU factorization with Orthomin[23] acceleration was used.

The material balance error was about 10^{-5} at the end of the simulation, which is certainly adequate for practical purposes. Note that the average degree of implicitness is only 11%. Recall that the NAPL pressure is always solved implicitly, but for this example, on average, only 11% of

Table III. Physical data for the three-dimensional DNAPL example

		Layer	Absolute permeabilities ($K_x = K_y = K_z$)
ρ_w	$100\ kg\ m^{-3}$	1,2	$10^{-14}\ m^2$
ρ_n	$1200\ kg\ m^{-3}$	3	$10^{-12}\ m^2$
μ_w	1·0 cP	4	$10^{-11}\ m^2$
μ_n	1·0 cP	5	$10^{-10}\ m^2$
ϕ	0·3	6	$10^{-12}\ m^2$
		7,8	$10^{-13}\ m^2$
		9	$10^{-14}\ m^2$
		10	$10^{-18}\ m^2$

Table IV. Relative permeability and capillary pressure tables used in the three-dimensional DNAPL example

NAPL–water data				Liquid-air data				
S_w	K_{rw}	K_{rn}	P_{cnw} (kPa)	$1 - S_a$	K_{ra}	K_{rna}	P_{can} (kPa)	P_{caw} (kPa)
0·2	0·0	0·68	9·0	0·2	0·64	0·0	9·0	6·6
0·3	0·04	0·55	5·4	0·32	0·46	0·0	3·0	4·5
0·4	0·10	0·43	3·9	0·40	0·36	0·0009	0·24	3·9
0·5	0·18	0·31	3·3	0·50	0·25	0·045	2·1	3·6
0·6	0·30	0·20	3·0	0·60	0·16	0·116	1·8	3·3
0·7	0·44	0·12	2·7	0·70	0·09	0·210	1·5	3·0
0·8	0·60	0·05	2·4	0·80	0·04	0·34	1·2	2·0
0·9	0·80	0·0	1·5	0·90	0·01	0·49	0·90	1·0
1·0	1·0	0·0	0·0	1·0	0·0	0·68	0·0	0·0
						$S_n^* = 0.1$ (see equation (6))		

Table V. Run statistics for the three-dimensional DNAPL problem

Number of nodes	3250
Number of tetrahedra	15552
Non-zero transmissibilities	19984
Negative transmissibilities	5424
Number of time steps	31
Total Newton iterations	208
Total inner iterations	1044
Average degree of implicitness	0·11
Material balance error	9×10^{-6}
Time reached	5 years
CPU time (MIPS/120 M)	3200 s

the nodes have the NAPL saturation S_n implicit as well. This is typical of contamination problems, since $S_n \equiv 0$ everywhere initially and mobile NAPL usually occurs only in a fraction of the total number of nodes.

Figures 5–7 show the simulation results at 5 years. The left side of the diagrams shows the values of the DNAPL saturation for each layer, while the right-hand side depicts the location of the nodes for that layer (i.e. the layer surface). The location of the DNAPL source can be clearly

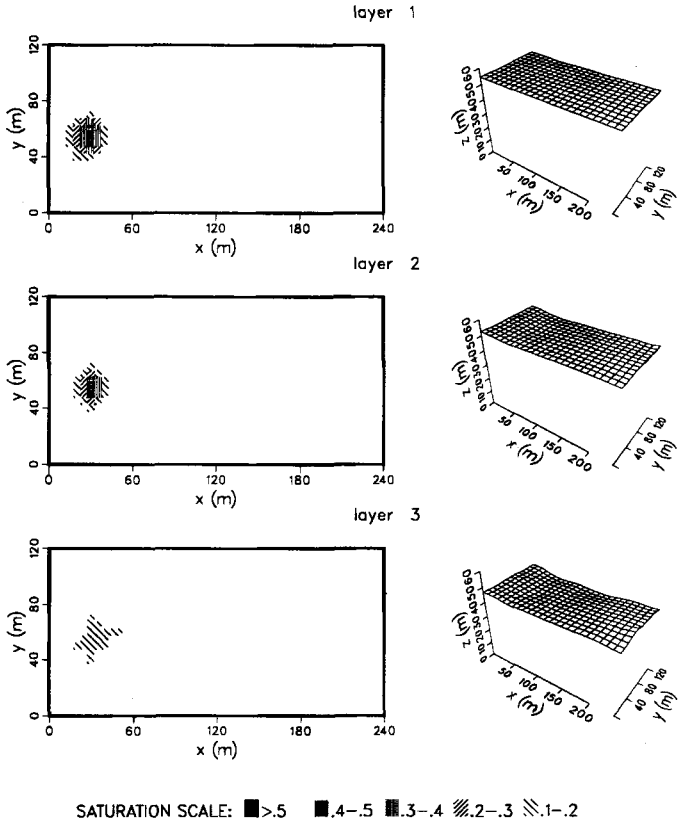

Figure 5. DNAPL saturation and layer surfaces for layers 1–3, full three-dimensional example

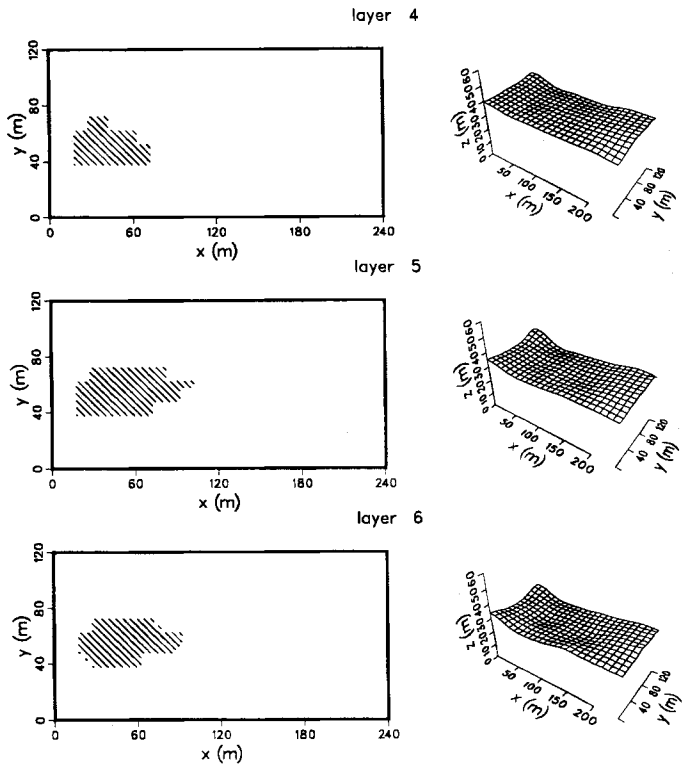

Figure 6. DNAPL saturation and layer surfaces for layers 4–6, full three-dimensional example

seen in layer 1 at the location of the large saturation values. There is a complicated interaction between the shape of the layer surface and the permeability contrast between a given layer and the one beneath it. For example, the permeability of layer 5 is two orders of magnitude larger than the permeability of layer 6 (see Table III). In this case we see that the DNAPL pools to a certain extent in layer 5. A finger of DNAPL then forms and moves towards the lowest point in layer 5. Since layer 10 is virtually impermeable, the DNAPL also pools in layer 9. Layer 10 is not shown since the DNAPL saturation is identically zero in this layer.

Unlike LNAPL contamination ($\rho_n < \rho_w$), where the water table is a barrier to contaminant migration, DNAPL will continue to flow downwards under the action of gravity. Even if an impermeable layer is encountered, DNAPL will continue to move along the layer to the lowest point. Consequently, DNAPL contaminant can be expected to move far from the original site of the spill. This makes remediation and clean-up of DNAPL sites extremely difficult.

An attempt was made to run this same problem with the five-tetrahedra decomposition of the blocks. This results in an order-of-magnitude increase in the size of the negative transmissibilities. The Newton iteration failed repeatedly, and excessively small time steps were required. As a result, we did not attempt to complete the simulation with this type of triangulation.

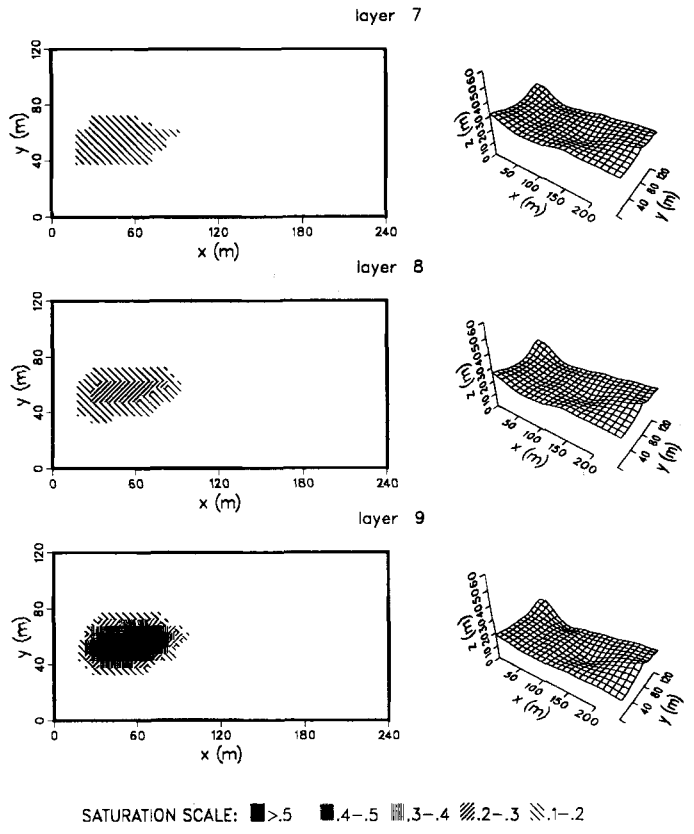

Figure 7. DNAPL saturation and layer surfaces for layers 7–9, full three-dimensional example

8. CONCLUSIONS

For both physical and computational reasons it is desirable to develop discretization methods having positive transmissibilities. Positive transmissibilities imply that the discrete fluid is in the same direction as the physical fluid flow.

A common technique for discretization of three-dimensional unsaturated grids is to use brick-type elements with 27-node connectivity. However, for grids typical of geophysical problems, brick-type elements give rise to a large number of negative transmissibilities.

Tetrahedra are the natural extension to three dimensions of triangles, which have been successfully used in two-dimensional problems.[18] Regions which are typical of NAPL contaminant simulation can be conveniently triangulated by first defining deformed blocks and then dividing the blocks into tetrahedra. There are essentially two ways to decompose blocks into tetrahedra, using either five or six tetrahedra.

It was demonstrated that the six-tetrahedra decomposition process produces negative transmissibilities which are smaller in (absolute) size than those of the five-tetrahedra decomposition for grids typical of geophysical problems. Numerical tests comparing the five- and six-tetrahedra methods showed that negative transmissibilities can have a pronounced effect on the Newton iteration. In particular, large negative transmissibilities result in non-physical flow paths, which can cause oscillations in the Newton iteration.

In general, unlike in two dimensions, it is not possible to eliminate negative transmissibilities without node movement. Node movement is undesirable, since the placement of nodes corresponds to the physically relevant geological layers. However, the six-tetrahedra block decomposition does give small negative transmissibilities for typical grid geometries.

Note that, on average, the use of tetrahedra results in 15-node connectivity. This is an advantage over larger node connectivity, since the amount of fill for a given level of incomplete factorization is proportional to the number of non-zeros (not the bandwidth) in the original matrix. Consequently, small node connectivity reduces the work required for the iterative solution of the Jacobian. If the discretization produces all positive transmissibilities, then in the single-phase incompressible limit the Jacobian becomes an M-matrix, which has excellent properties for iterative solvers.

Simulation of a realistic NAPL contamination scenario required only a small number of fully implicit nodes on average. Consequently, the adaptive implicit method, coupled with an iterative matrix solver, permits the solution of fairly large three-dimensional problems with modest requirements in terms of computational work and storage.

REFERENCES

1. C. Faust, 'Transport of immiscible fluids within and below the unsaturated zone', *Water Resources Res.*, **21**, 587–596 (1985).
2. M. Osbourne and J. Sykes, 'Numerical modelling of immiscible organic transport in the Hyde Park landfill', *Water Resources Res.*, **22**, 25–33 (1986).
3. L. M. Abriola and G. F. Pinder, 'A multiphase approach to the modelling of porous media contamination by organic compounds 1. Equation development', *Water Resources Res.*, **21**, 11–18 (1985).
4. L. M. Abriola and G. F. Pinder, 'A multiphase approach to the modelling of porous media contamination by organic compounds 2. Numerical simulation', *Water Resources Res.*, **21**, 19–26 (1985).
5. G. F. Pinder and L. M. Abriola, 'On the simulation of nonaqueous phase organic compounds in the subsurface', *Water Resources Res.*, **22**, 109S–119S (1986).
6. P. A. Forsyth, 'Simulation of nonaqueous phase groundwater contamination', *Adv. Water Resources*, **11**, 74–83 (1988).
7. C. R. Faust, J. H. Guswa and J. W. Mercer, 'Simulation of three dimensional flow of immiscible fluids within and below the unsaturated zone', *Water Resources Res.*, submitted for publication.
8. T. Kuppusamy, J. Sheng, J. Parker and R. Lenhard, 'Finite element analysis of multiphase immiscible flow through soils', *Water Resources Res.*, **23**, 625–631 (1987).
9. J. Kaluarachchi and J. Parker, 'An efficient finite element method for modelling multiphase flow', *Water Resources Res.*, **25**, 43–54 (1989).
10. P. S. Huyakorn and G. F. Pinder, *Computational Methods in Subsurface Flow*, Academic, New York, 1983.
11. K. Aziz and A. Settari, *Petroleum Reservoir Simulation*, Applied Science, London, 1979.
12. P. A. Forsyth, 'Comparison of the single phase and two phase numerical model formulation for saturated–unsaturated groundwater flow', *Comput. Methods Appl. Mech. Eng.*, **69**, 243–259 (1988).
13. C. Prakesh, 'Examination of the upwind formulation in the control volume finite element method for fluid flow and heat transfer', *Numer. Heat Transfer*, **11**, 401–416 (1987).
14. P. A. Forsyth, 'A control volume finite element method for local mesh refinement', *SPE J. Reservoir Eng.*, **5**, 561–566 (1990).
15. R. Bank and D. Rose, 'Some error estimates for the box method', *SIAM J. Numer. Anal.*, **24**, 777–787 (1987).
16. P. S. Huyakorn, S. D. Thomas and B. M. Thompson, 'Techniques for making finite element methods competitive in modelling flow in variably saturated porous media', *Water Resources Res.*, **20**, 1099–1115 (1984).
17. P. H. Sammon, 'An analysis of upstream differencing', *SPEJ. Reservoir Eng.*, **3**, 1053–1056 (1988).
18. P. A. Forsyth, 'A control volume finite element approach to NAPL groundwater contamination', *SIAM J. Sci. Stat. Comput.*, to appear (1991).
19. B. Joe, 'Delauney triangular meshes in convex polygons', *SIAM J. Sci. Stat. Comput.*, **7**, 514–539 (1986).
20. F. W. Letniowski, 'Three dimensional Delauney triangulations for finite element approximations to a second order diffusion operator', *SIAM J. Sci. Stat. Comput.*, to appear (1992).
21. P. A. Forsyth and P. H. Sammon, 'Practical considerations for adaptive implicit methods in reservoir simulation', *J. Comput. Phys.*, **62**, 265–281 (1986).
22. P. A. Forsyth, 'Adaptive implicit criteria for two phase flow with gravity and capillary pressure', *SIAM J. Sci. Stat. Comput.*, **10**, 227–252 (1989).
23. A. Behie and P. A. Forsyth, 'Incomplete factorization methods for fully implicit enhanced oil recovery', *SIAM J. Sci. Stat. Comput.*, **5**, 543–561 (1984).
24. A. Bermon and P. Plemmons, *Non Negative Matrices in the Physical Sciences*, Academic, New York, 1979.